Original Article

Institution of MECHANICAL ENGINEERS
Journal of MULTI-BODY DYNAMICS

Proc IMechE Part K:
J Multi-body Dynamics
2015, Vol. 229(3) 245–258

DOI: 10.1177/1464419314559078
pik.sagepub.com
SAGE

Development and verification of a multi-body dynamic model for seat-occupant system of manned spacecraft

Ali Akbar Pasha Zanoosi[1], Mohammadreza Mallakzadeh[2] and Reza Kalantarinejad[3]

Abstract

The main goal of this study is to develop a novel multi-body dynamic model for seat-occupant system of a manned spacecraft. The seat of a spacecraft and its components has significant effects on an astronaut's body during flight mission, where sustained accelerations and impact loads are inevitable. Besides, conducting sustained acceleration and shock loads on the body of astronauts during flight missions is the key factor for health conservation. This study develops a new multi-body dynamic model for seat-occupant system of manned spacecraft to investigate the effects of spacecraft seat design. The astronaut is modelled as a four-jointed rigid link placed on a viscoelastic cushion. The cushion is modelled to present polyurethane foam, which is using in almost all automotive and aerospace applications. The equations of motion are derived and the effects of different parameters are investigated. To verify the developed model, a finite element model is presented to implement the same exact multi-body model. The results show that the presented analytical multi-body model is in good accordance with the finite element model. The effects of different parameters such as foam discretisation, foam thickness and geometry of seat frame on the motion of the system are illustrated. This novel model can be used in designing spacecraft seat to preserve an astronaut's health. It also can be used in seat control applications and where computational efficiency is necessary.

Keywords

Spacecraft, seat-occupant system, multi-body model, polyurethane foam, viscoelastic materials, VUMAT subroutine

Date received: 18 May 2014; accepted: 10 October 2014

Introduction

Seats are one of the most important components of manned system vehicles and seating is one of the most critical components to be considered during design of such vehicles. Seats are the final interface between the occupant and the vehicle. Especially in a spacecraft, all launch and landing operations are performed through seats. Significant effort must be spent to ensure proper integration of the human to the spacecraft.

During re-entry step of a flight mission, direction and magnitude of acceleration of the vehicle produce a resultant acceleration vector of different direction and magnitude when coupled with the increasing effects of gravity. This acceleration vector is unique to each seat position and the occupant seated in the vehicle. When altering the seat's pitch, roll and yaw, each of these factors changes the linear and rotational acceleration vector profiles that the seat will undergo and can markedly affect the ability of the seat occupant's to tolerate the acceleration profile and/or perform critical functions.[1]

In most historical examples of spacecraft, this results in the crew being seated recumbently for landing.

In the case of seats, the acceleration energy should either be removed or sufficiently managed by the

[1]School of Mechanical Engineering, Iran University of Science and Technology, Iran
[2]Biomechanics Group, School of Mechanical Engineering, Iran University of Science and Technology, Iran
[3]Astronautics Research Institute, Iranian Space Research Centre, Iran

Corresponding author:
Mohammadreza Mallakzadeh, Biomechanics Group, School of Mechanical Engineering, Iran University of Science and Technology, Narmak, Tehran
16846-13114, Iran.
Email: mmallak@iust.ac.ir

system to allow for occupant survival. To allow flexibility for risk analysis, NASA has most recently employed a whole-body acceleration exposure limit method, as characterized by the predicted dynamic response of the seated occupant to a given input acceleration of the system.[2] Using this model, the systems designer can account for landing or abort accelerations from the point of application to the vehicle, through all structures, and ultimately to the occupant through his or her seat.

Landing impact is inevitable during manned missions. When the manned airdrop equipment descends to an Earth landing by parachute, the astronauts are exposed to the ground impact forces.[3] Previous studies[4–7] have demonstrated that human body can tolerate certain levels of landing impact forces but the high-level impact forces may have a disadvantageous influence on the human body and even endanger the lives of astronauts. Therefore, the landing technologies of the manned spacecrafts have been extensively researched.

To study human responses to impact forces, many impact experiments have been conducted.[8–10] Brown et al.[11] simulated 24 body positions and conducted 288 experiments that were likely to occur during the landing of Apollo command model. The study demonstrated that humans could endure certain predicted Apollo landing impact forces in different body orientations without significant injury or undue pain. Stapp and Taylor[12] conducted a series of impact experiments using the rocket sled and summarized human tolerance to deceleration. The results indicated that all the body positions and impact configurations were within human tolerance limits except the forward-facing 45° reclining position. Liu et al.[13] reported astronaut dynamic responses to landing impact at different segments in selected body positions. Cheng et al.[14] studied human tolerance limitation in sitting position and showed that human body can tolerate the acceleration peak of $14\,g$ during 50 ms. In the experiments, the human dynamic responses were correlated with the acceleration peak, duration and body position. Once these responses exceeded human tolerance limitations, the astronauts would suffer serious injuries. It should be noted that these experiments considered the body position as an important factor of an astronaut's dynamic responses.

In the actual landing impact, not only the body position but also the positions of other parts have significant effects on human injuries. Hence, understanding an astronaut's body dynamic responses seems a more important problem, which is beneficial to design a safe and secure seat.

Through this process, the relative simplicity and effectiveness of the acceleration-induced injury risk model must be considered along with its limitations. While it is relatively easy to apply for the seat and vehicle designers, this model has an inherent limitation in that it remains valid only when the underlying assumptions and test conditions upon which it was built remain intact. To this aim, modelling the seat-occupant system of manned spacecraft is mandatory.

There are mainly three types of models for seat-occupant systems. These are based on the modelling technique used: lumped parameter models, multi-body models and finite element models (FEM).

Multi-body models can be used in more than one dimension and are able to predict quantities and responses that cannot be measured, compared with lumped parameter models. They are able to describe the effects of global deformations with high computational efficiency as compared with FEM and do not need as many inputs. Despite their advantages, multi-body models, especially in more than one dimension, have not been used widely, although there are a few models described in the literature, such as those developed by Nishiyama.[15–17] All these models are applied in automotive applications and it should be mentioned that there is no such model for aerospace applications.

The seat characteristics play an important role in the response of the seated occupants to input loads. For example, most modern car seats are full-foam (flexible polyurethane foam); thus the properties of foam significantly affect the static and dynamic comfort of occupants. Hence, it is important to develop models of seat-occupant systems that incorporate the properties of the foam.[18] Although there are a number of studies that measure the response of humans in seated position to excitation applied to the base of a rigid seat, only in the past few years have researchers started measuring and modelling the response to humans seated on soft seats, thus introducing the effects of the seating foam. The study by Hinz et al.[19] deals with the measurement of the apparent mass of human subjects on a soft seat with a backrest cushion, while the study by Patten et al.[20] involves measuring and modelling the response of a human seated on an automotive seat cushion with a single degree-of-freedom model. Cho and Yoon[21] use a multi-body model to describe the measured transmissibility with backrest support. As has been mentioned previously, all these models have found applications in automotive industries.

The goal of this study is the development of a multi-body modelling approach that can predict the response of the seated occupant in a manned spacecraft to changing occupant and seat characteristics such as frame geometry and foam thickness. Such a model will have the ability to predict the static and dynamic responses of the seated occupant during flight mission and for different exposed loads. The developed model will be able to predict the biodynamic responses of seated occupants to excitations applied at the seat frame. This research presents a two-dimensional, multi-body seat-occupant model of a manned spacecraft system for predicting the static equilibrium position of the occupant in the seat. The modelling approach incorporates rigid body dynamics of the occupant, large deformation

viscoelastic models of the flexible polyurethane foam in unidirectional compression and a model of the forces at the seat-occupant interface. The foam accommodated between the seat frame and the occupant is represented by a number of unidirectional nonlinear viscoelastic elements. The resulting multi-degree-of-freedom system's analytical model is developed using Lagrangian formulation. To verify the developed model, an FEM has been developed that is similar to the multi-body model. To model the polyurethane foam behaviour, a hand-written Fortran code is employed and imported in finite element software to present the exact same behaviour of mathematical foam model. The results from multi-body model and FEM show very good agreement. Finally the effects of seat parameters, such as foam thickness and seat geometry, on occupant dynamic response are shown using different figures.

Seat-occupant system and multi-body model development

The different elements of modelled seat-occupant system are shown in Figure 1. The polyurethane foam shown in Figure 1 is assumed to be represented by a number of equivalent nonlinear viscoelastic spring and damper elements. The parameters of these springs depend on the properties of the seating foam and are defined by the constitutive model of the foam described later.

Besides, forces in interfacial surfaces of seat and occupant are considered in normal and tangential directions. The occupant model is presented by four rigid links describing head and neck, femur, shank and trunk, as shown in Figure 1.

Constitutive foam model

Available evidences recommend the use of rate-dependent foams in operational seat cushions assuming that these foams are reasonably durable and suitable for operational use. Such cushions have the potential to enhance long-term sitting comfort and to improve the impact protection performance of escape systems in high-performance aircrafts and spacecrafts.

Flexible polyurethane foam is used in automotive and aerospace seating. The stress–strain relationship of this foam is highly nonlinear and depends on the strain rate, as seen from the stress–strain curve of foam obtained from a uniaxial cyclic compression test.[18] Flexible polyurethane foam is highly nonlinear and has viscoelastic characteristics; hence, its effects on the complex dynamic response of the seat-occupant system can be applied by considering a single degree-of- freedom system in uni-directional motion.[18]

The properties of foam depend on the foam compression because the stiffness of foam changes with compression level. Also, there is a substantial difference in the loading and unloading curves due to the viscoelasticity and other dissipation mechanisms present in foam. The model of the behaviour of foam in uni-directional compression (for a single-cycle test) is assumed to be given by the following stress–strain relation

$$\sum_{j=1}^{M} k_j \varepsilon^j + \int_0^t \sum_{i=1}^{N} a_i e^{-\alpha_i (t-\tau)} \dot{\varepsilon}(\tau) \mathrm{d}\tau = F(t)/A \qquad (1)$$

The first term represents the nonlinear elastic stress component, with the nonlinear form defined by a polynomial through 'stiffness' parameters, while the second term is the viscoelastic stress component dependent on the strain rate. The strain ε is defined as $\varepsilon = H - x/H$.[18] The nonlinear elastic and linear viscoelastic parameters for the seating foam is taken from the study of Gauri et al.[18]

The seating foam is assumed to be made up of a sufficient number of these nonlinear viscoelastic spring elements. This is an approach to model the behaviour of the seat-occupant system, where the

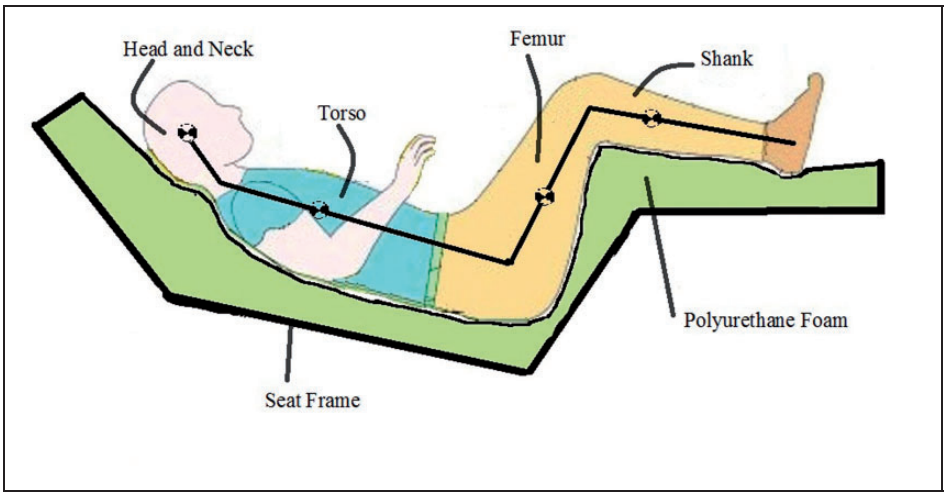

Figure 1. Different elements of seat-occupant model.

material properties are an integral part of the model and the influence of changes in the material behaviour on the occupant responses can be directly examined using this model. In this sense, this model is based on physical modelling of the components and not a response-driven model.

Seat-occupant multi-body model

The considered model for occupant is composed of four primary elements representing head and neck, femur, trunk and shank. The geometric parameters are depicted is Figure 2.

For more accurate modelling, head and neck are separated from the trunk. Six generalized coordinates are considered as follows: ζ, η, θ_1, θ_2, θ_3 and θ_4.

The origin of inertia coordinate is shown as point A on the frame (Figure 2). Figure 3 shows the inertia parameters of each segment.

Modelling spring-damper elements

In the presented model, seat cushion is modelled as several discretized spring-damper elements. One end of each element moves along the occupant but it is restricted to be orthogonal to each body part. The other end is attached to the seat frame.

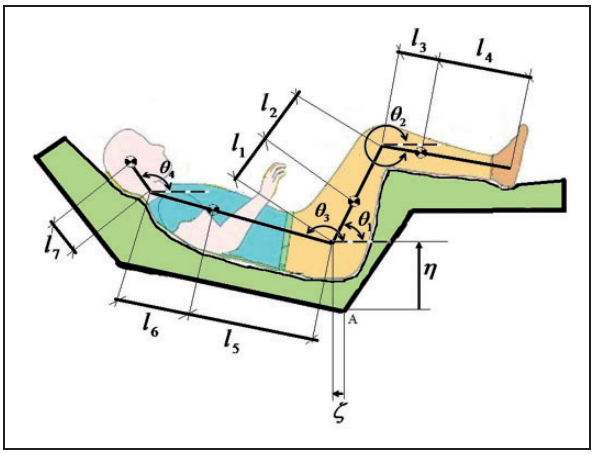

Figure 2. The occupant model: geometric parameters and configuration.

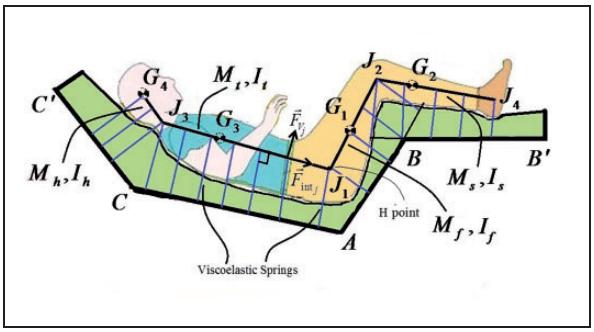

Figure 3. The position of centre of masses and joints of the occupant. Inertia parameters for describing system motion and the position of hip joint and nonlinear viscoelastic elements. $\vec{F}_{\text{int}_j}$ and $\vec{F}_{V_j}$ are the j^{th} element interfacial and viscoelastic forces, respectively.

Seat cushion has been considered as several nonlinear viscoelastic springs in different parts. Besides, forces in the interfacial surface of foam and occupant have two tangential and normal components.

The occupant model involves head–neck, trunk, femur and shank. Seat frame in composed of four segments corresponding to each occupant part. The hip joint position and the position of discretized spring elements are shown in Figure 3.

Seat cushion is considered as several discretized spring elements, which models the viscoelastic and nonlinear elastic behaviour of foam, according to equation (1). It should be noted that there is no connection between these individual elements and accordingly the resulting shear in the contact is not considered. The discrete nature of the elements can be justified by noting that for soft material, the significant part of contact deformation occurs locally, with minimal deformation effect remotely from each element; this is shown by the column method contact mechanics approach.[22]

It is also worth mentioning that the contact is subject to accelerative input; therefore it suffers shock loading. In fact, the instantaneous generated contact pressures penetrate into the seat and occupant body in waveforms with a series of frequencies. The constituents with lower frequency penetrate further.[23] Since implementing the above-mentioned features in the system makes the problem computationally expensive, in this study, the developed simplified model is a preliminary step into decreasing the computational costs and increasing the efficiency of the model.

The foam force computed from equation (1) predicts the foam force accurately for compression levels between 0% and 70%. This foam force has to be modified so that the force exerted by foam as compression approaches 100% tends towards infinity.[24]

At very high compression levels, the polyurethane structure at microscopic level is attended (i.e. the air is squeezed out of the foam) and the polyurethane strut elements are in contact with each other. As compression increases, the polyurethane material itself becomes compressed. Thus, at very high compression levels, there is an exponential-like increase in the foam force. Also, the foam force should be 0 for all compression levels less than 0% because the seated occupant loses contact with the foam when compression becomes 0 and seat-occupant interaction does not support tension in foam. Ippili et al.[25] modified the predicted spring force by two sigmoid functions

$$S_1 = 1/\left(1 + e^{250(1-\varepsilon-0.98)}\right) \tag{2}$$

$$S_2 = 1/\left(1 + e^{-125(1-\varepsilon-0.1)}\right) \tag{3}$$

Multiplication with the first sigmoid function S_1 makes the force 0 if the strain <0. Dividing the force by the second sigmoid function S_2 makes the force $\rightarrow \infty$ when strain is >0.90.

The spring elements are assumed to be attached to the occupant and are constrained to remain perpendicular to the body. There is no dissipation or resistance at the joints of the occupant, all dissipation being modelled through the viscoelastic foam model and linear dampers associated with each nonlinear viscoelastic spring.

Modelling of interfacial forces

The in-plane forces at the seat-occupant interface are included in the model. The interfacial forces between the occupant and the seat, including the frictional and the tangential shear forces, play an essential role in determining the static settling point for the system. These forces are important to prevent the occupant from sliding out of seat. Very few researchers have reported on the characterization of the occupant-seat interface. This interface is extremely complex due to the number of layers of materials and the interfacial properties of these materials. To take these interfacial forces into account, here a crude approximation by a simple model has been assumed.

In this study, it is assumed that these forces act on the occupant tangentially at the points where the viscoelastic spring forces act normally. Accordingly, it is assumed that the interfacial forces act on the occupant at the points where the spring forces act. These spring forces represent the interaction between the seat cushion and the occupant. Furthermore, these forces are tangential to the body in a direction opposite to the motion of the body at that point and have magnitude proportional to the spring force F. Thus, the force at a given point is

$$F_{\text{int}} = -\mu |F| \tag{4}$$

This model represents the maximum friction force and the orientation of each interface force vector is then always parallel to the occupant's body component at the point of attachment of the spring.

Equations of motion

The equations of motion for the seat-occupant system can be derived by using Lagrangian formulation.[26] The Lagrangian formulation simplifies the task of writing down equations for the complex seat-occupant system. In this study, a base excitation $Z(t)$ in the vertical direction and $X(t)$ in the horizontal direction is applied to the system. The Lagrangian formulation consists of n second-order differential equations that define the motion of a system with n generalized coordinates. The Lagrange's equations of motion for a system are given by

$$\frac{d}{dt}\left(\frac{\partial T}{\partial \dot{q}_r}\right) - \frac{\partial T}{\partial q_r} + \frac{\partial U}{\partial q_r} + \frac{\partial D}{\partial \dot{q}_r} = Q_r, \quad r = 1, 2, \ldots, n \tag{5}$$

$D(\dot{q}_r)$ is used for representing the energy dissipated due to linear velocity proportional damping. The kinetic energy, the potential energy, the generalized forces and the Raleigh dissipation function for the seat-occupant system are given by

$$T = \frac{1}{2}\sum_{i=1}^{4} m_i\left(\dot{x}_1^2 + \dot{z}_1^2\right) + \frac{1}{2}\sum_{i=1}^{4} I_i\left(\dot{\theta}_i^2\right) \tag{6}$$

$$U = g\sum_{i=1}^{4} m_i Z_i + \sum_{i=1}^{n_{total}} V_i(\delta_i) \tag{7}$$

$$Q_i = \sum_{j=1}^{n_{total}} \vec{F}_{\text{int}\,j} \cdot \frac{\partial \vec{r}_j}{\partial q_i} + \sum_{j=1}^{n_{total}} \vec{F}_{V\,j} \cdot \frac{\partial \vec{r}_j}{\partial q_i} \tag{8}$$

In the above equations, $i = 1, 2, 3, 4$ can be head–neck, trunk, femur and shank. The centre of mass of the head and neck, the femur and the shank and trunk can be defined in terms of the generalized coordinates

$$\begin{aligned}
&A_x = X(t)\, Base\, Movement\, (Input),\\
&A_y = Z(t)\, Base\, Movement\, (Input)\\
&J_{1x} = X(t) + \zeta(t),\ J_{1y} = Z(t) + \eta(t),\\
&J_{2x} = J_{1x} + (l_1 + l_2)\cos(\theta_1),\ J_{2y} = J_{1y} + (l_1 + l_2)\sin(\theta_1)\\
&J_{3x} = J_{1x} + (l_5 + l_6)\cos(\theta_3),\ J_{3y} = J_{1y} + (l_5 + l_6)\sin(\theta_3)\\
&J_{4x} = J_{2x} + (l_3 + l_4)\cos(\theta_2),\ J_{4y} = J_{2y} + (l_3 + l_4)\sin(\theta_2)\\
&G_{1x} = J_{1x} + l_1\cos(\theta_1),\ G_{1y} = J_{1y} + l_1\sin(\theta_1),\\
&G_{2x} = J_{2x} + l_3\cos(\theta_2),\ G_{2y} = J_{2y} + l_3\sin(\theta_2)\\
&G_{3x} = J_{1x} + l_5\cos(\theta_3),\ G_{3y} = J_{1y} + l_5\sin(\theta_3),\\
&G_{4x} = J_{3x} + l_7\cos(\theta_4),\ G_{4y} = J_{3y} + l_7\sin(\theta_4).
\end{aligned} \tag{9}$$

where $Z(t)$ and $X(t)$ are the displacement of the seat base due to the external vertical and horizontal excitation applied at the seat base. The defined terms for the foam potential and dissipation energy in the equations of motion are given by

$$\begin{aligned}
U &= \sum_{i=1}^{n_{total}} V_i(\delta_i) = \int_0^{\delta} \sum_{i=1}^{n_{total}} F_i(\delta_i)\, \mathrm{d}\delta_i\\
UV_\delta(r) &= \frac{\partial U_v}{\partial q_r} = \frac{\partial}{\partial q_r}\int_0^{\delta} \sum_{i=1}^{n_{total}} F_i(\delta_i)\, \mathrm{d}\delta_i\\
&= \sum_{i=1}^{n_{total}} F_i(\delta_i)\frac{\partial \delta_i}{\partial q_r}; \quad \delta = \delta(q_r)
\end{aligned} \tag{10}$$

$$D = \frac{1}{2}\sum_{i=1}^{n_{total}} c_i \dot{\delta}_i^2,\ D_\delta = \frac{\partial D}{\partial \dot{q}_r} \tag{11}$$

$M_{total} = M_f + M_s + M_h + M_t$ and $n_{total} = n_f + n_s + n_h + n_t$. For the term Q_i, it should be noted that the tangential forces act along centre line of each segment and the viscoelastic forces are normal to the segments. For tangential and viscoelastic forces, which are non-conservative, the generalized forces are given by

$$Q_i = Q_i^{\text{int}} + Q_i^V = \sum_{j=1}^{n_{total}} \vec{F}_{\text{int}\,j} \cdot \frac{\partial \vec{r}_j}{\partial q_i} + \sum_{j=1}^{n_{total}} \vec{F}_{V\,j} \cdot \frac{\partial \vec{r}_j}{\partial q_i} \tag{12}$$

Finally, substituting the above equations in Lagrange equations, the equations of motion can be derived as

$$[M]\{\ddot{Q}\} = [A] \tag{13}$$

where M is a 6 by 6 matrix and its arrays are

$$\begin{aligned}
&M_{11} = M_{total},\ M_{12} = 0,\\
&M_{13} = -M_f l_1 \sin(\theta_1) - M_s(l_1 + l_2)\sin(\theta_1)\\
&M_{14} = -M_s l_3 \sin(\theta_2),\\
&M_{15} = -M_t l_5 \sin(\theta_3) - M_h(l_5 + l_6)\sin(\theta_3)\\
&M_{16} = -M_h l_7 \sin(\theta_4),\ M_{21} = 0,\ M_{22} = M_{total}\\
&M_{23} = M_s(l_1 + l_2)\cos(\theta_1) + M_f l_1 \cos(\theta_1),\\
&M_{24} = M_s l_3 \cos(\theta_2)\\
&M_{25} = M_h(l_5 + l_6)\cos(\theta_3) + M_t l_5 \cos(\theta_3),\\
&M_{26} = M_h l_7 \cos(\theta_4)\\
&M_{31} = -\big(M_f l_1 \sin(\theta_1) + M_s(l_1 + l_2)\sin(\theta_1)\big)\\
&M_{32} = M_f l_1 \cos(\theta_1) + M_s(l_1 + l_2)\cos(\theta_1)\\
&M_{33} = I_f + M_f l_f^2 + M_s(l_1 + l_2)^2\\
&M_{34} = M_s l_3(l_1 + l_2)(\cos(\theta_2 - \theta_1))\\
&M_{35} = 0,\ M_{36} = 0,\ M_{41} = -M_s l_3 \sin(\theta_2),\\
&M_{42} = M_s l_3 \cos(\theta_2)\\
&M_{43} = M_s l_3(l_1 + l_2)(\cos(\theta_2 - \theta_1)),\ M_{44} = I_2 + M_s l_3^2\\
&M_{45} = 0,\ M_{46} = 0,\ M_{51} = -(M_t l_5 + M_h l_5 + M_h l_6)\sin(\theta_3)\\
&M_{52} = (M_t l_5 + M_h l_5 + M_h l_6)\cos(\theta_3),\ M_{53} = 0,\ M_{54} = 0\\
&M_{55} = I_t + M_t l_6^2 + M_h(l_5 + l_6)^2,\\
&M_{56} = M_h l_7(l_5 + l_6)\cos(\theta_4 - \theta_3)\\
&M_{61} = -M_h l_7 \sin(\theta_4),\ M_{62} = M_h l_7 \cos(\theta_4),\\
&M_{63} = 0, M_{64} = 0\\
&M_{65} = M_h l_7(l_5 + l_6)\cos(\theta_4 - \theta_3),\ M_{66} = M_h l_7^2
\end{aligned} \tag{14}$$

$\ddot{Q}$ includes the second derivative of generalized coordinates as

$$\ddot{Q} = \begin{bmatrix} \ddot{\xi} & \ddot{\eta} & \ddot{\theta}_1 & \ddot{\theta}_2 & \ddot{\theta}_3 & \ddot{\theta}_4 \end{bmatrix}^T \tag{15}$$

Also, A involves the following terms

$$\begin{aligned}
A(1) &= \Delta_\zeta + M_{total}\ddot{X} - \big(M_s(l_1 + l_2) + M_f l_1\big)\cos(\theta_1)\dot{\theta}_1^2\\
&\quad - M_s l_3 \dot{\theta}_2^2 \cos(\theta_2)\\
&\quad - (M_t l_5 + M_h l_5 + M_h l_6)\dot{\theta}_3^2 \cos(\theta_3)\\
&\quad - M_h l_7 \dot{\theta}_4^2 \cos(\theta_4)\\
A(2) &= \Delta_\eta + M_{total}\big(\ddot{Z} + g\big)\\
&\quad - \big(M_f l_1 + M_s l_1 + M_s l_2\big)\dot{\theta}_1^2 \sin(\theta_1)\\
&\quad - M_s l_3 \dot{\theta}_2^2 \sin(\theta_2) - (M_t l_5 + M_h l_5 + M_h l_6)\dot{\theta}_3^2 \sin(\theta_3)\\
&\quad - M_h l_7 \dot{\theta}_4^2 \sin(\theta_4)\\
A(3) &= \Delta_{\theta_1} - \big(M_s l_2 + M_s l_1 + M_f l_1\big)\\
&\quad \times \big(\ddot{X}\sin(\theta_1) + \big(g + \ddot{Z}\big)\cos(\theta_1)\big)\\
&\quad + M_s l_3(l_1 + l_2)\sin(\theta_1 - \theta_2)\dot{\theta}_2^2\\
A(4) &= \Delta_{\theta_2} + M_s l_3\big(-\sin(\theta_2)\ddot{X} + \big(\ddot{Z} + g\big)\cos(\theta_2)\\
&\quad + (l_1 + l_2)\sin(\theta_2 - \theta_1)\dot{\theta}_1^2\big)\\
A(5) &= \Delta_{\theta_3} - (M_t l_5 + M_h l_5 + M_h l_6)\\
&\quad \times \big(\sin(\theta_3)\ddot{X} + \big(\ddot{Z} + g\big)\cos(\theta_3)\big)\\
&\quad + M_h l_7(l_5 + l_6)\sin(\theta_3 - \theta_4)\dot{\theta}_4^2\\
A(6) &= \Delta_{\theta_4} - M_h l_7\big(\sin(\theta_4)\ddot{X} - \big(g + \ddot{Z}\big)\cos(\theta_4)\\
&\quad + (l_5 + l_6)\sin(\theta_3 - \theta_4)\dot{\theta}_3^2\big)
\end{aligned} \tag{16}$$

where the Δ terms in above equation are

$$\begin{aligned}
\Delta_\zeta &= UV_\delta(1) + D_\delta(1) + Q(1)\\
\Delta_\eta &= UV_\delta(2) + D_\delta(2) + Q(2)\\
\Delta_{\theta_1} &= UV_\delta(3) + D_\delta(3) + Q(3)\\
\Delta_{\theta_2} &= UV_\delta(4) + D_\delta(4) + Q(4)\\
\Delta_{\theta_3} &= UV_\delta(5) + D_\delta(5) + Q(5)\\
\Delta_{\theta_4} &= UV_\delta(6) + D_\delta(6) + Q(6)
\end{aligned} \tag{17}$$

Single-degree-of-freedom foam-block model

The force $F(\delta_i)$ (equation 10) consists of non-linear elastic and linear viscoelastic components. Therefore, $F(\delta_i) = A[\sigma_e(X_i) + \sigma_v(X_i)]$. The linear viscoelastic component $\sigma_v(X_i)$ is represented by the integral in equation (1) and can be expressed as

$$F_v(t) = \int_{-\infty}^{t} \sum_{i=1}^{N} a_i e^{-\alpha_i(t-\tau)} x(\tau)\mathrm{d}\tau \tag{18}$$

For a two-term viscoelastic model ($N = 2$) Singh[26] showed that the integral in equation (18) can be converted into a differential equation of the form

$$\begin{aligned}
\ddot{F}_v &= (a_1\alpha_2 + a_2\alpha_1)x + (a_1 + a_2)\dot{x}\\
&\quad - \alpha_1\alpha_2 F_v - (\alpha_1 + \alpha_2)\dot{F}
\end{aligned} \tag{19}$$

Thus equation (18) has been transformed into a differential equation.

For a seat-occupant system with n_{total} springs, there will be n_{total} differential equations like equation (19) that have to be solved in conjunction with the second-order differential equations represented in matrix form by equation (19). Therefore, if viscoelastic effects are considered, as the number of springs used to represent the foam increases, the number of second-order differential equations to be solved also increases. Therefore, it results in a significant increase in the computational time required to numerically integrate these equations.

Seat-occupant FEM

To verify the developed multi-body model, the FEM of the seat-occupant system has been practiced. Four-jointed rigid links with the same inertia properties has been modelled to represent occupant in recumbent position. The occupant is located on a deformable material representing seat cushion. The FEM in an arbitrary initial state is shown in Figure 4.

The special behaviour and mathematical model of the viscoelastic polyurethane foam (equation 1) considered in this study led to using material models in ABAQUS. It should be noted that there is no material model corresponding the viscoelastic foam applied as seat cushion in the software. Therefore, to regenerate the same mathematical model, a VUMAT subroutine in Fortran is written to produce the same mathematical model as equation (1).

The finite element modelling of viscoelastic behaviour has been widely reported in the literature. The vast majority, however, deals with the isotropic case, where there are only two distinct sets of relaxation behaviour: one associated with the shear modulus and the other with bulk modulus.

The original algorithm of Poon and Ahmad[27] addresses linear viscoelasticity. The key algebraic structure and the basic steps in the algorithmic development are general enough to accommodate non-linear viscoelastic behaviour, at least in the form proposed by Schapery.[28]

Focusing on the computational task at hand and adding superscripts to indicate the time step, the constitutive law can be re-written as

$$\sigma_{ij}^{n+1} = h_e^{n+1}\left[\sum_k \sum_l C_{ijkl}^{\infty}\bar{\varepsilon}_{kl}^{n+1}\right] + h_1^{n+1}\sum_k \sum_l \left[\tilde{C}_{ijkl}h_2^{n+1}\bar{\varepsilon}_{kl}^{n+1} - D_{ijkl}^{n+1}\right] \quad (20)$$

The only unknown on the right-hand side is D_{ijkl}^{n+1}.

User is free to choose an appropriate method for integrating equation (1). The backward Euler scheme is implemented here for ease of coding. Alternate strategies such as the generalized trapezoidal rule can be adopted easily.

Replacing the derivative by finite difference in equation (1), and using the backward Euler scheme, which is known for its stability, the following can be obtained[29]

$$D_{ijkl}^{n+1} = \left(\frac{1}{\Delta t} + \frac{1}{\tau_{ijkl}A_{ijkl}^{n+1}}\right)^{-1}\left[\frac{D_{ijkl}^{n}}{\Delta t} + \frac{\tilde{C}_{ijkl}h_2^{n+1}\bar{\varepsilon}_{kl}^{n+1}}{\tau_{ijkl}A_{ijkl}^{n+1}}\right] \quad (21)$$

Consistent tangent operator

The consistent tangent operator concept was introduced by Simo and Taylor[30] in the context of rate-independent plasticity. During the incremental

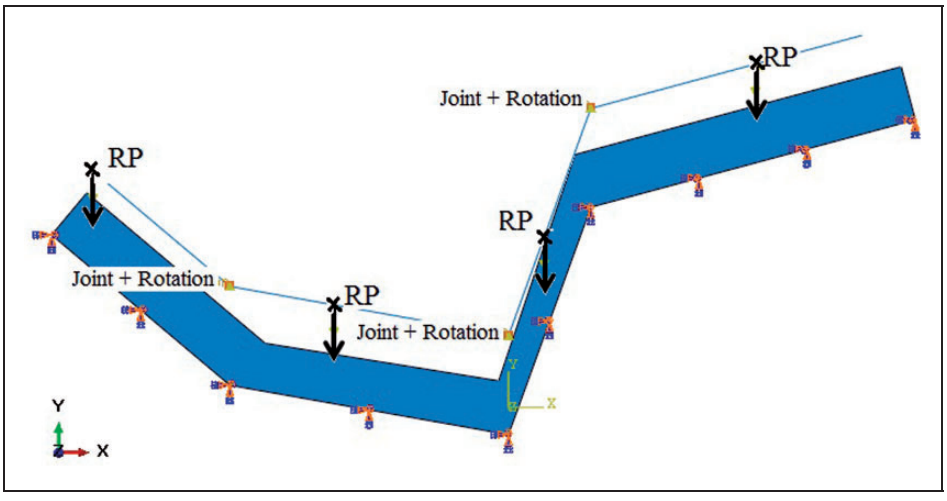

Figure 4. The corresponding finite element model of developed multi-body model.
RP: Reference Point.

solution process for non-linear problems, non-linear virtual work equations are solved by Newton's method. In updating the global Jacobian matrix, estimates are needed, at the integration point level, of the rate of change of stress with regard to strain. Previously, the quantities $\partial\dot{\sigma}/\partial\dot{\varepsilon}$ were used, resulting in sub-optimal convergence rates. It turns out that using the quantity $\partial\sigma^{n+1}/\partial\Delta\varepsilon$ produces better results because this expression depends not only on the constitutive law but also on the time integration algorithm in the constitutive update.

The use of this quantity preserves the quadratic convergence rate of Newton's method and accelerates the search for displacement fields that best satisfies the principle of virtual work.

From the study of Poon and Ahmad,[29] the consistent tangent operator required in VUMAT subroutines is

$$\begin{aligned}\frac{\partial\sigma_{ij}^{n+1}}{\partial\Delta\varepsilon_{ab}} &= h_e C_{ijab}^{\infty} + \frac{\partial h_e}{\partial\Delta\varepsilon_{ab}}\left[\sum_k\sum_l C_{ijkl}^{\infty}\bar{\varepsilon}_{kl}^{n+1}\right] \\ &+ \frac{\partial h_1}{\partial\Delta\varepsilon_{ab}}\sum_k\sum_l\left[\tilde{C}_{ijkl}h_2\bar{\varepsilon}_{kl}^{n+1} - D_{ijkl}^{n+1}\right] \\ &+ h_1h_2\tilde{C}_{ijab} - h_1h_2G_{ijab} \\ &+ h_1\frac{\partial h_2}{\partial\Delta\varepsilon_{ab}}\left[\sum_k\sum_l C_{ijkl}\bar{\varepsilon}_{kl}^{n+1}\right] \\ &- h_1\frac{\partial h_2}{\partial\Delta\varepsilon_{ab}}\left[\sum_k\sum_l G_{ijkl}\bar{\varepsilon}_{kl}^{n+1}\right] \end{aligned} \tag{22}$$

where

$$G_{ijkl} = \left(\frac{1}{\Delta t} + \frac{1}{\tau_{ijkl}A_{ijkl}^{n+1}}\right)^{-1}\frac{\tilde{C}_{ijkl}}{\tau_{ijkl}A_{ijkl}^{n+1}} \tag{23}$$

In equation (22), quantities such as h_e, h_1 and h_2, as well as their partial derivatives, are to be evaluated at the end of the increment. The corresponding terms has been substituted in these equations to be representative of viscoelastic polyurethane foam in this study.

Results and discussion

The occupant has been modelled as four-jointed rigid links with mass and inertia moments. The seat frame dictates the geometry of the seat, which is modelled as a rigid body with fixed geometry. The seat cushion is assumed to be a viscoelastic material. The viscoelastic cushion material in this study is considered to be polyurethane foam. The foam has been modelled as several discretized spring-damper elements. The interaction of the foam and the occupant occurs through two tangential and normal force components. The equations of motion have been derived and simulation results are presented in this section.

For simulation sake, the anthropometric parameters for an astronaut weighing 75 kg and 180 cm in height have been used. The anthropometric data (centres of gravity, moment of inertia and mass distribution) are taken from the study of Winter.[31]

To verify the developed multi-body model, an FEM is developed. The polyurethane foam with its specific strain–stress mathematical behaviour is imported through a hand-written code. The results for some specific cases are shown in this section. Considering $\psi_1 = 70^\circ$, $\psi_2 = 15^\circ$, $\psi_3 = 170^\circ$ and $\psi_4 = 140^\circ$ and friction coefficient $\mu = 0.25$ for all segments and initial thickness of foam as $h_0 = 10$ cm, the simulation results from developed multi-body model and FEM for the following initial condition are presented in Figures 5–10

$$\begin{aligned} Q^0 &= \begin{bmatrix}\zeta^0 & \eta^0 & \theta_1^0 & \theta_2^0 & \theta_3^0 & \theta_4^0\end{bmatrix}^T \\ &= \begin{bmatrix}1 & 1.3h_0 & \psi_1 & \psi_2 & \psi_3 & \psi_4\end{bmatrix}^T \end{aligned} \tag{24}$$

To choose the best number of spring elements, first the results obtained from multi-body model are

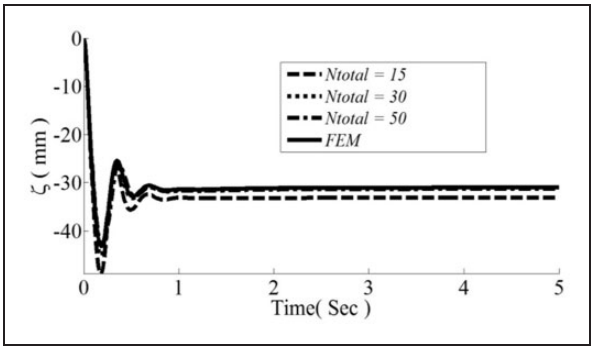

Figure 5. Comparison between multi-body and FEM and effects of number of springs on ζ.
FEM: finite element model.

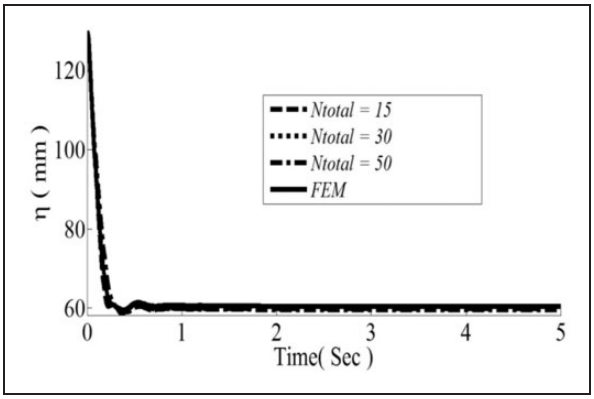

Figure 6. Comparison between multi-body and FEM and effects of number of springs on η.
FEM: finite element model.

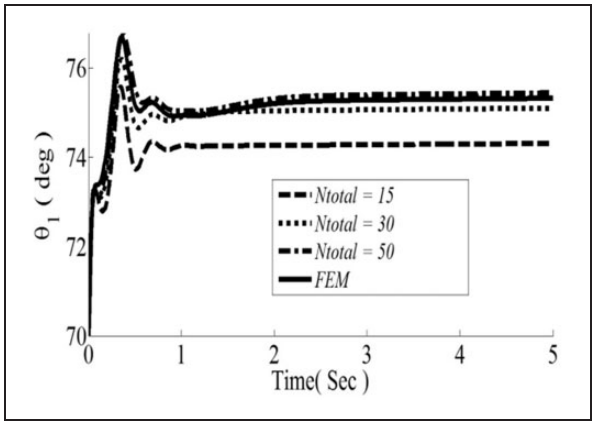

Figure 7. Comparison between multi-body and FEM and effects of number of springs on θ_1.
FEM: finite element model.

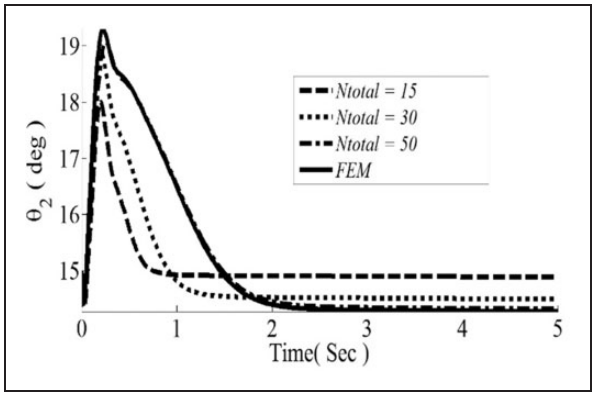

Figure 8. Comparison between multi-body and FEM and effects of number of springs on θ_2.
FEM: finite element model.

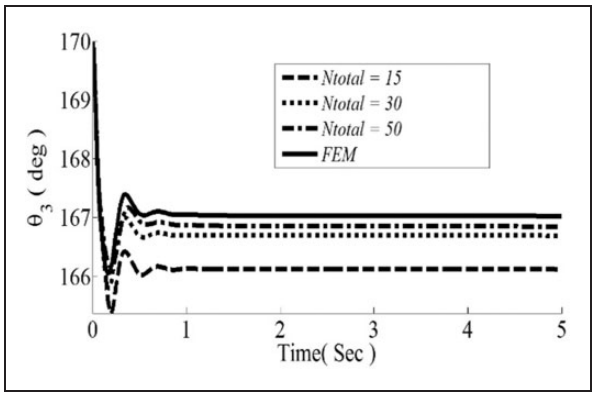

Figure 9. Comparison between multi-body and FEM and effects of number of springs on θ_3.
FEM: finite element model.

compared with those from FEM. The results in Figures 5–10 show good agreement between the developed multi-body model and FEM. Results also show the good convergence of the motion of system

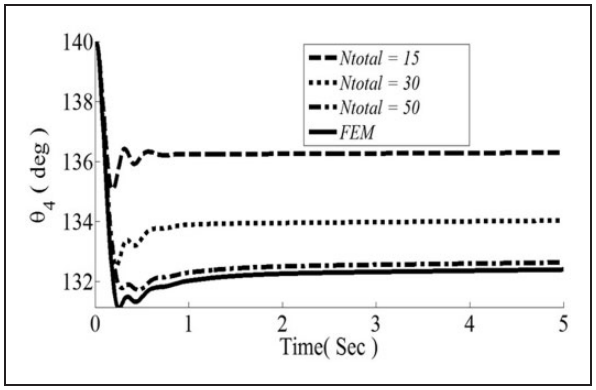

Figure 10. Comparison between multi-body and FEM and effects of number of springs on θ_4.
FEM: finite element model.

regarding variation of number of discretized spring elements.

Figures 5–10 illustrate the response of the system for an arbitrary initial condition. The results are represented for different numbers of seat cushion discretized elements. According to these figures, as the number of cushion discretized elements increases, the results obtained from multi-body model converge with the results of FEM. The results of multi-body model are in a very good agreement with the results of finite elements, which certify the accuracy of the presented multi-body model. For $N = 50$, the results of multi-body model reveal appropriate agreement with FEM results. However, it should be mentioned that increasing the number of discretization corresponds with increasing the total number of differential equations that should be solved. This means that the total number of discretized elements is chosen in a way that both computational efficiency and model accuracy are preserved. Here $N = 50$ satisfies these two aims.

Figure 11 shows the strains in discretized elements during the motion. The marked lines in the figure determine the strain within different discretized viscoelastic elements.

The viscoelastic forces are as shown in Figure 12. Viscoelastic materials have some time-dependent features. They reveal their features with time. The cushion is a viscoelastic material. Whenever gravity has an effect, it shows its time integration properties. The marked lines in Figure 12 determine the viscoelastic forces in different discretized spring elements.

The thickness of the foam (h_0) has significant effects on the response of the occupant. Large thicknesses would make large displacements of the occupant and small thicknesses would expose high loads to the occupant, which increases injury potentials. The effects of foam thickness on the response of the occupant are shown in the following figures.

According to Figures 13–18, the changes in foam thickness cause changes in the motion of the system,

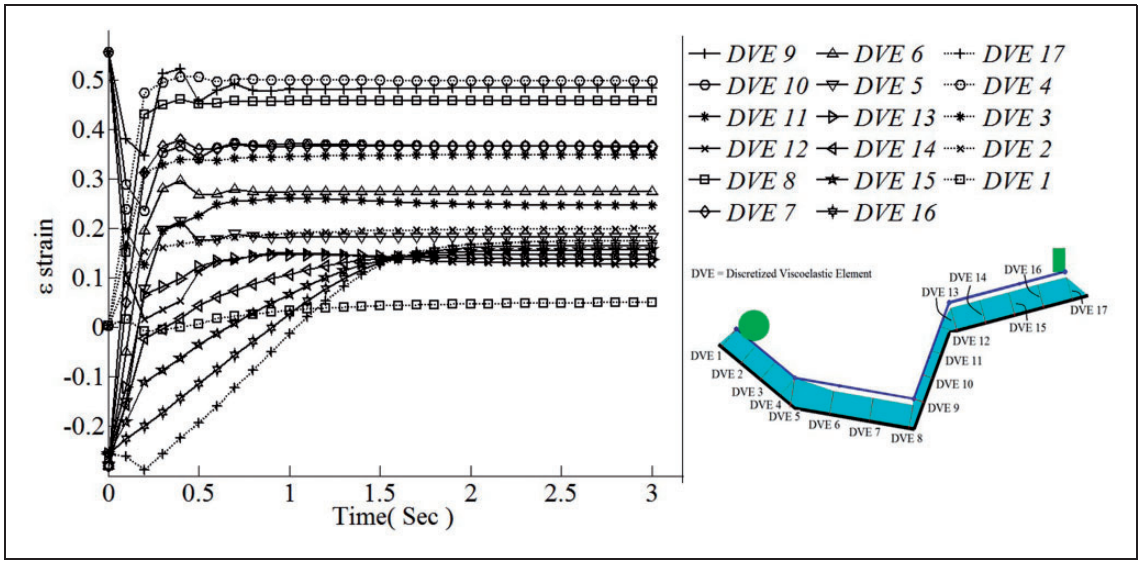

Figure 11. Strain in viscoelastic spring elements of the foam.
DVE: discretized viscoelastic element.

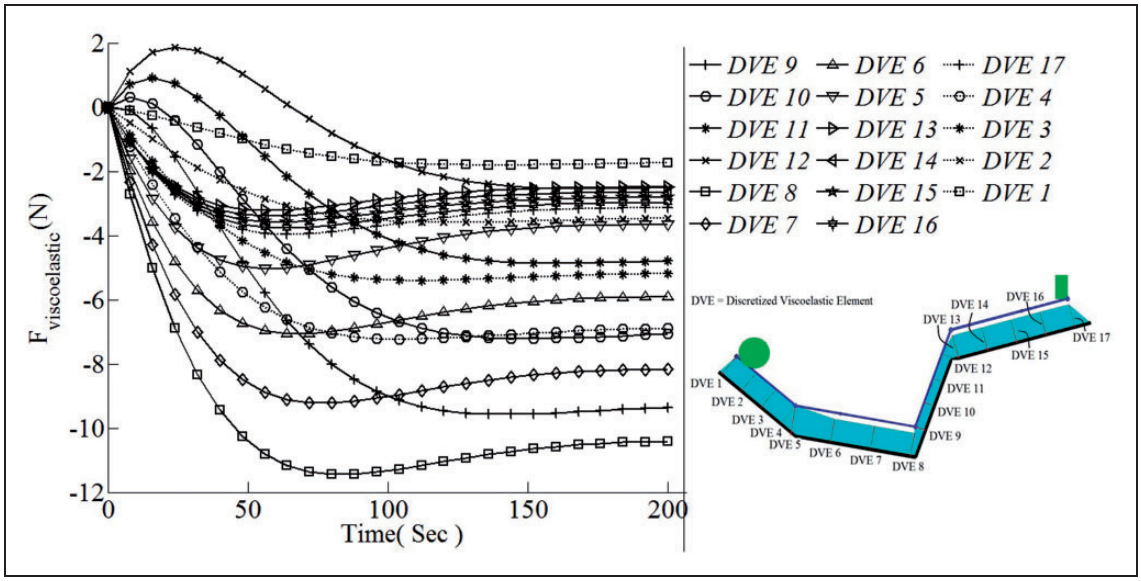

Figure 12. Viscoelastic Forces in viscoelastic spring elements of the foam.
DVE: discretized viscoelastic element.

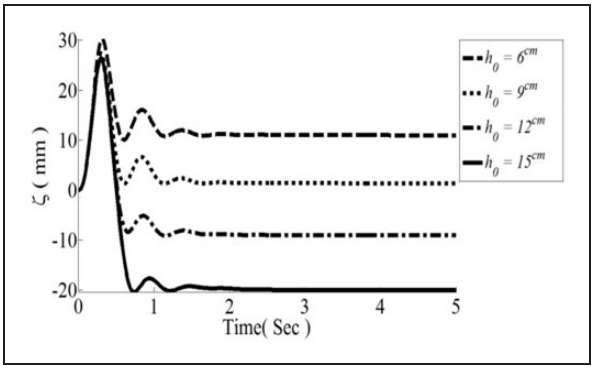

Figure 13. Effect of foam thickness on ζ.

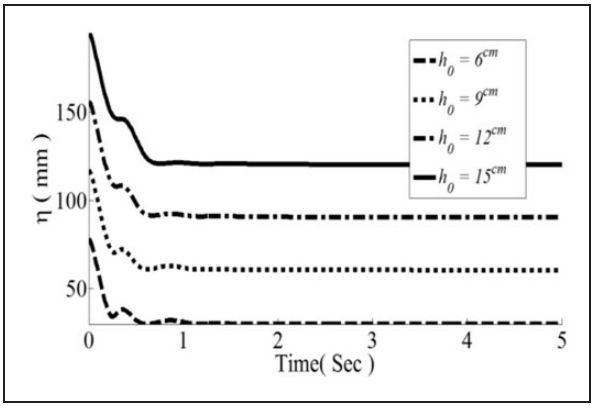

Figure 14. Effect of foam thickness on η.

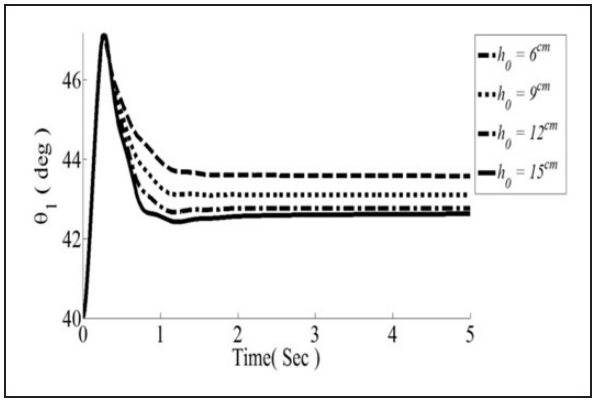

Figure 15. Effect of foam thickness on θ_1.

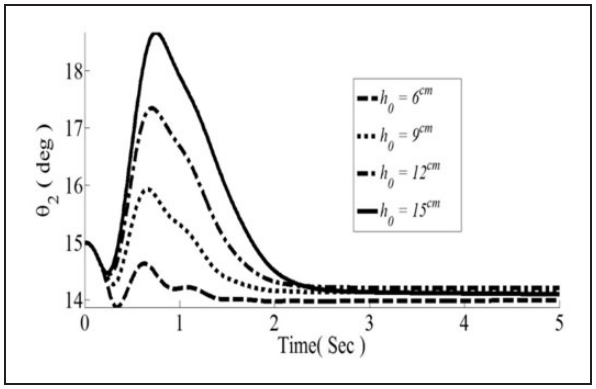

Figure 16. Effect of foam thickness on θ_2.

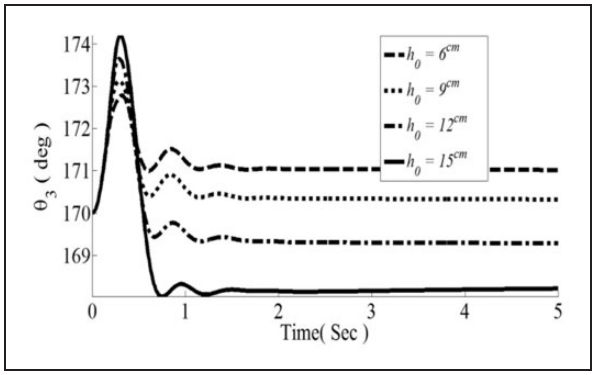

Figure 17. Effect of foam thickness on θ_3.

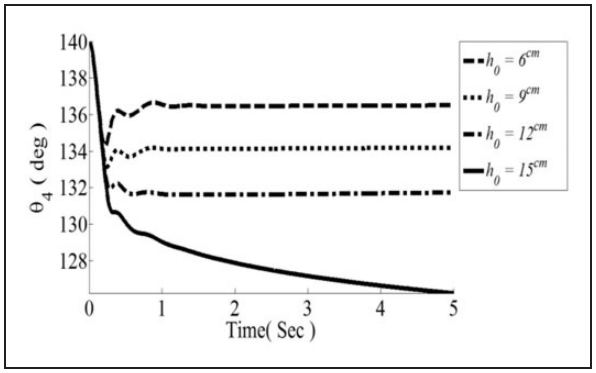

Figure 18. Effect of foam thickness on θ_4.

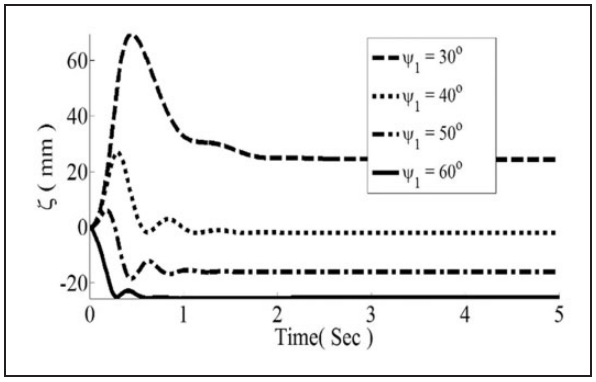

Figure 19. Effect of changes in ψ_1 on ζ.

especially in the angles of body parts. As Figures 13 and 14 show, the displacement of hip joint is changing by variation in cushion thickness. The hip joint displacement results in whole body movement. The effects of the foam thickness on body parts movement is also shown in Figures 15–18. It is shown that increasing the cushion thickness leads to increase in occupant motion. Furthermore, decreasing the cushion thickness also leads to different motion in occupant body movements. Therefore, designers should consider these effects based on the goals that they are looking for.

As it is mentioned before, the development of multi-body models help designers to design their desired parameters based on their goal, more accurately and efficiently. In spacecraft seats, the aim is to decrease the probable injury to an astronaut to its lowest level. To achieve this, the response of an astronaut's body has to be predicted. The obtained results of this study continues with the investigation on the effects of seat geometry on the occupant response.

To investigate the effects of seat geometry on the dynamic response of an occupant, the effects of changes in the seat frame geometry, i.e. ψ_1, ψ_2, ψ_3 and ψ_4 on occupant motion are illustrated.

Effects of ψ_1 on hip joint movement is shown in Figures 19 and 20. Increasing ψ_1 causes the decrease of both horizontal and vertical motions of hip joint.

Effects of ψ_2 on hip joint location movements are shown in the figure below.

Figures 21 and 22 clearly show that changes in ψ_2 have small effects on the hip joint motions.

Changes in ψ_3, which corresponds to the place of trunk, have significant effects on system movements. As Figure 23 shows, changes in this parameter lead to sudden motion on horizontal location of the hip joint. The final position of this joint is lowered as

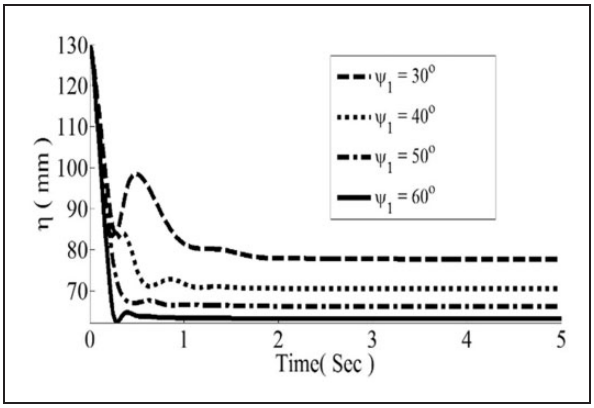

Figure 20. Effect of changes in ψ_1 on η.

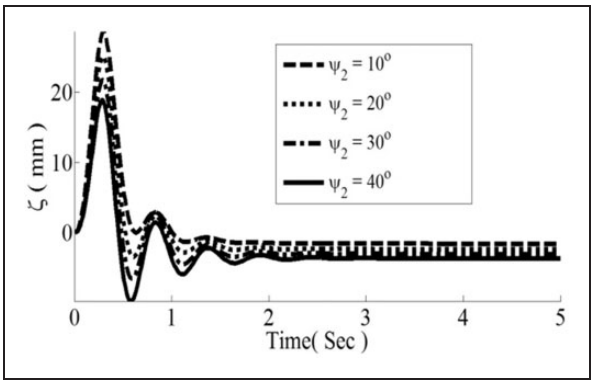

Figure 21. Effect of changes in ψ_2 on ζ.

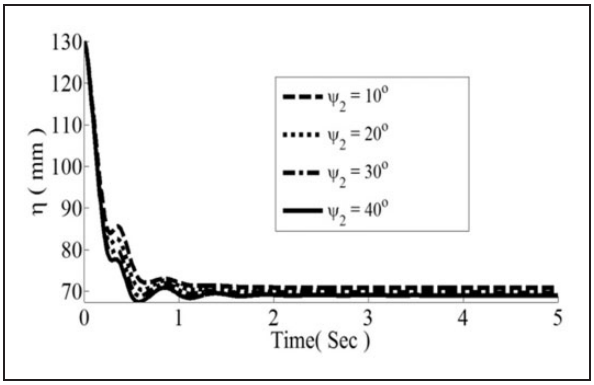

Figure 22. Effect of changes in ψ_2 on η.

ψ_3 increases. The effects of ψ_3 on θ_2 are shown in Figure 24. The changes in the motion of θ_2 are significantly affected by ψ_3.

The effects of all these parameters can be investigated, separately. Developing this multi-body model with computational efficiency provides the possibility to analyze these effects in a more reasonable computational time and makes it possible to conduct high computational procedures such as optimization algorithms.

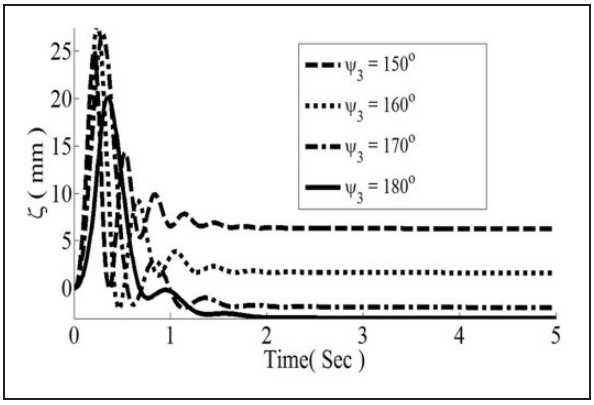

Figure 23. Effect of changes in ψ_3 on ζ.

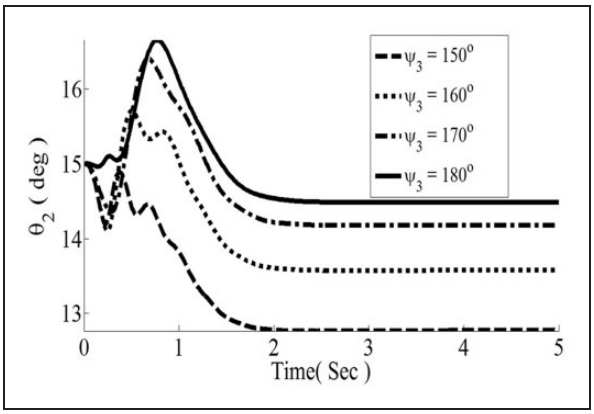

Figure 24. Effect of changes in ψ_3 on η.

Conclusions

The aim of this study was to develop a novel multi-body dynamic model for predicting dynamic behaviour of the seat-occupant system of manned spacecraft. Among different engineering models, multi-body models are well known for high computational efficiency and ease of implementation.

Motion prediction of astronaut's body response to dynamic load during flight mission and especially during landing makes designer to be aware of susceptible parts of body which injury potential is more likely. These predictions make it possible to design the seat with secure injury risks through seat geometry and proper seat cushion. It also makes it possible to control the attitude of seat in a way that keeps the astronaut in a safe configuration.

A four-segment multi-body model of occupant is considered through this study to model the seat-occupant system of a manned spacecraft. The system is composed of seat frame, seat cushion and occupant. The derived equations of motion are verified by the same FEM.

The effects of foam discretization has been compared with FEM results to show the convergence of foam discretized model. The results also illustrate the effects of seat cushion thickness, foam discretzation

and seat frame geometry on dynamic behaviour of an astronaut's body. The results show high efficiency, accuracy and applicability of the developed model. This computationally effective model can be used to survey the motion of the system and the effects of involved parameters. These results are important in designing the seat of spacecrafts to guarantee safety of astronauts.

Conflict of interest

None declared.

Funding

This research received no specific grant from any funding agency in the public, commercial, or not-for-profit sectors.

References

1. Gohmert DM. Seating considerations for *spaceflight: the human to machine interface*. Houston, TX: NASA Johnson Space Center, 2012.
2. Gohmert DM, Stroud K, Locke J, et al. *Crew exploration vehicle DAC 1A seat layout study white paper*. JSC-65230. Houston, TX: NASA Johnson Space Center, 2006.
3. Homma T and Saltelli A. Importance measures in global sensitivity analysis of nonlinear models. *Reliab Eng Syst Saf* 1996; 52: 1–17.
4. Lawrence C, Carney KS and Littell J. Astronaut risk levels during crew module (CM) land landing. NASA/TM-2007-214669, 2007.
5. Wang YL. Analysis of human tolerance to landing impact of manned spacecraft. *Space Med Med Eng (Beijing)* 1996; 9(1): 60–63.
6. Wang YL, Luo J, Cheng ZL, et al. Experimental study of injury characteristics of +Gx landing impact. *Space Med Med Eng (Beijing)* 1994; 7(3): 157–162.
7. Weis EB, Clarke NP and Brinkley JW. Human response to several impact orientations and patterns. *Aerosp Med* 1963; 34: 1122–1129.
8. Do S and de Weck OL. A personal airbag system for the Orion crew exploration vehicle. *Acta Astronaut* 2012; 81: 239–255.
9. Du HL, Huang SL and Zhang JH. Study on evaluation guideline and injury factor of head, neck, thorax and vertebra during high G landing impact. *Chin J Clin Rehabil* 2004; 8: 1474–1475.
10. Liu BK, Ma HL, Jiang SZ, et al. Simulation analysis of human neck injury risk under high-level landing impact. *Int J Crashworthiness* 2008; 14(6): 585–590.
11. Brown WK, Rothstein JD and Foster LP. Human response to predicted Apollo landing impacts in selected body orientations. *Aerosp Med* 1966; 37(4): 394–398.
12. Stapp JP and Taylor ER. Space cabin landing impact vector effects on human physiology. *Aerosp Med* 1964; 35: 1117–1132.
13. Liu BK, Ma HL and Jiang SZ. Dynamic responses to landing impact at different key segments in selected body positions. *Aerosp Sci Technol* 2008; 12: 331–336.
14. Cheng ZL, Han YF, Zeng WY, et al. Human tolerance to landing impact (+Gz) in sitting position. *Space Med Med Eng (Beijing)* 1997; 10(5): 340–343.
15. Nishiyama S. Development of simulation system on vehicle occupant dynamic interaction: 1st report, theoretical analysis and system verification. *Trans Japan Soc Mech Eng C* 1993; 59: 3613–3621.
16. Nishiyama S. Development of simulation system on vehicle occupant dynamic interaction: 2nd report, influence of sitting posture on human comfort. *Trans Japan Soc Mech Eng C* 1993; 59: 3622–3629.
17. Nishiyama S. Development of simulation system on vehicleoccupant dynamic interaction: 3rd report, influence of parameters of occupant-seat system on human comfort. *Trans Japan Soc Mech Eng C* 1994; 60: 1509–1516.
18. Gauri J, Bajaj AK and Davies P. Whole-body vibratory response study using a nonlinear multi-body model of seat-occupant system with viscoelastic flexible polyurethane foam. *Ind Health* 2010; 48: 663–674.
19. Hinz B, Rützel S, Blüthner R, et al. Apparent mass of seated man—first determination with a soft seat and dynamic seat pressure distributions. *J Sound Vib* 2006; 289: 704–724.
20. Patten W, Sha S and Mo C. A vibrational model of open celled polyurethane foam automotive seat cushions. *J Sound Vib* 1998; 217: 145–161.
21. Cho Y and Yoon YS. Biomechanical model of human on seat with backrest for evaluating ride quality. *Int J Ind Ergonom* 2001; 27: 331–345.
22. Rahnejat H. Multi-body dynamics: historical evolution and application. *Proc IMechE, Part C: J Mechanical Engineering Science* 2000; 214(1): 149–173.
23. Teodorescu M, Rahnejat H, Gohar R, et al. Harmonic decomposition analysis of contact mechanics of bonded layered elastic solids. *Appl Math Model* 2009; 33: 467–485.
24. Ippili RK, Davies P, Bajaj AK, et al. Nonlinear multi-body dynamic modeling of seat–occupant system with polyurethane seat and H-point prediction. *Int J Ind Ergonom* 2008; 38: 368–383.
25. Yamada H. *Strength of biological materials*. Huntington, New York: Robert E Krieger Publishing Company, 1970.
26. Singh R. *Dynamic modeling of polyurethane foam and development of system identification methodologies*. MS Thesis, Purdue University, West Lafayette, IN, 2000.
27. Poon H and Ahmad MF. A material point time integration procedure for anisotropic, thermo rheologically simple, viscoelastic solids. *Comp Mech* 1998; 21: 236–242.
28. Schapery RA. On the characterization of non-linear viscoelastic materials. *Polym Eng Sci* 1969; 9: 295–310.
29. Poon H and Ahmad MF. A finite element constitutive update scheme for anisotropic, viscoelastic solids exhibiting non-linearity of the Schapery type. *Int J Numer Meth Eng* 1999; 46: 2027–2041.
30. Simo JC and Taylor RL. Consistent tangent operators for rate-independent elastoplasticity. *Comp Meth Appl Mech Eng* 1985; 48: 101–118.
31. Winter DA. *Biomechanics and motor control of human movement*. 4th ed. New York: John Wiley, 2009.

Appendix

Notation

a_i	foam viscoelastic parameter
A	area of the foam normal to the direction of loading

$D(\dot{q}_r)$	Rayleigh dissipation function
$F(t)$	force acting on the foam
$\vec{F}_{\text{int } j}$	interfacial force at the j^{th} spring due to normal forces
H	the uncompressed height of the foam block
I_i	moment of inertia of the i^{th} body element about its center of mass
k_j	stiffness parameters of the foam
m_i	mass of the i^{th} body element
M_f, I_f	mass and inertia moment of femur
M_h, I_h	mass and inertia moment of head–neck
M_s, I_s	mass and inertia moment of shank
M_t, I_t	mass and inertia moment of trunk
M_{total}	total mass of occupant
n_f	number of springs at the femur
n_h	number of springs at the head–neck
n_s	number of springs at the shank
n_t	number of springs at the trunk
n_{total}	total number of discretized elements
q_r	generalized coordinates of the system.
$Q_r(q_r, \dot{q}_r, t)$	generalized forces
$T = T(q_r, \dot{q}_r)$	kinetic energy of the system
$U = U(q_r)$	potential energy of the system
$V_i(\delta_i)$	potential energy of the i^{th} spring
x	deformed height of the foam block
α_i	foam viscoelastic parameter
δ	compression of each spring
ε	strain in the foam
ζ	horizontal position of hip joint
η	vertical position of hip joint
θ_1	angular position of femur with respect to horizontal axis
θ_2	angular position of shank with respect to horizontal axis
θ_3	angular position of trunk with respect to horizontal axis
θ_4	angular position of head–neck with respect to horizontal axis